Size-Dependent Phase Diagram of Nanoscale Alloy Drops Used in Vapor−Liquid−Solid Growth of Semiconductor Nanowires

Eli A. Sutter* and Peter W. Sutter

Center for Functional Nanomaterials, Brookhaven National Laboratory, Upton, New York 11973

ABSTRACT We use *in situ* observations during high-temperature transmission electron microscopy to quantify the exchange of semiconductor material between Au−Ge vapor−liquid−solid seed drops and Ge nanowires (NWs). By performing simultaneous measurements under identical conditions on arrays with systematic variations in NW diameter, we establish the nanoscale size dependence of the temperature-dependent equilibrium composition of the Au−Ge binary alloy. We find a significantly enhanced Ge solubility for drops on thin NWs compared to thicker ones. The controlled modification of the surface of the NW by an ordered carbon shell leads to drastic changes in the solubility.

KEYWORDS: semiconductor nanowires · nanoscale phase diagrams · semiconductor−metal alloy drops · Au−Ge binary system · vapor−liquid−solid growth

Semiconductor nanowires (NWs), self-assembled nanostructures that can be prepared in high-yield processes[1−3] based on vapor−liquid−solid (VLS) growth,[4] have attracted a lot of interest for potential applications in nanoelectronics,[5] light emitters and detectors,[6] photovoltaics,[7−9] or thermoelectrics.[10,11] Central to the VLS NW growth process is the exchange of atoms of the semiconductor species between a liquid metal−semiconductor binary alloy seed drop and the growing NW. The properties of this system—the alloy melt drop in contact with the solid NW—at or close to thermodynamic equilibrium, represented by the phase diagram of the binary alloy, govern important aspects of VLS NW growth. A key parameter is the equilibrium composition of the alloy drop, whose temperature dependence is given by the liquidus line in the phase diagram. For a fixed amount of metal, the equilibrium composition of the seed drop defines the drop size, which determines the NW diameter[12,13] and in turn—*via* quantum confinement in thin NWs or band bending and surface depletion in thicker, bulk-like wires—the electronic structure of the wire.[14,15] The equilibrium composition also affects other important aspects of the growth, such as the supersaturation and the growth rate.

Given the small dimensions of typical NWs and their VLS alloy seed drops (few tens of nanometers), the known bulk phase diagrams cannot provide a reliable basis for predicting NW growth. We have recently reported the first measurements of the phase diagram of alloy drops on NWs, demonstrating that it deviates drastically from the bulk, and that knowledge of the actual phase diagram of the nanoscale VLS system is a powerful tool to judiciously tailor the geometry of a growing NW.[13] The phase behavior should be affected strongly by surface effects (*i.e.*, the excess energies due to the free surfaces of the drop and NW and the interface between them) and is expected to vary significantly with size. Theoretical calculations based on classical thermodynamic considerations, however, have come to conflicting conclusions, predicting either a significant size dependence of the phase diagrams (*e.g.*, for Au−Si and Au−Ge[16,17]) or only small deviations from the bulk phase behavior.[18,19] Here we use *in situ* microscopy experiments to establish the size-dependent phase diagram of nanoscale alloy drops, used as seeds in VLS growth, in equilibrium with a solid semiconductor NW. By variable-temperature transmission electron microscopy (TEM) on Au−Ge alloy drops at the tips of Ge NWs, key features of the phase diagram of the nanoscale alloy are determined. By performing these measurements simultaneously on arrays of NWs with systematic diameter variations, we are able to directly demonstrate significant size dependences in the

*Address correspondence to esutter@bnl.gov.

Received for review June 17, 2010 and accepted July 14, 2010.

Published online July 19, 2010.
10.1021/nn101366w

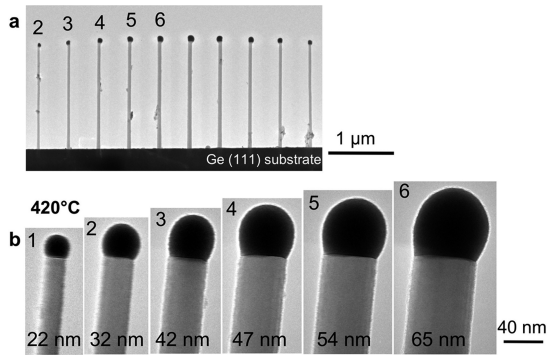

Figure 1. (a) Linear array of Ge NWs on the thinned original Ge substrate during the *in situ* TEM experiments. Numbers identify NWs with different diameters in one-half of the array. (b) TEM images showing individual Ge NWs from the array in panel a (identified by the same numbers) close to the Au−Ge alloy drop at the NW tip during *in situ* annealing at 420 °C. The NW diameters are given in each panel.

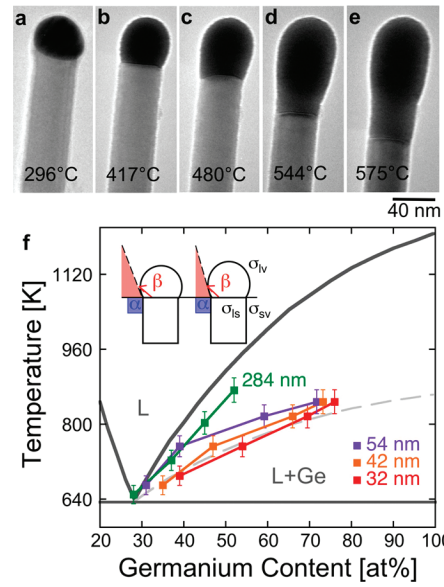

Figure 2. (a−e) Sequence of TEM images showing one of the Ge NWs (NW 3) from the linear array in Figure 1, close to the NW tip during *in situ* annealing at different temperatures between room temperature and 575 °C. (a) Au−Ge alloy crystalline nanoparticle adjacent to the Ge NW before surface melting starts; (b−e) exchange of material across the Ge NW/liquid drop interface after melting of the alloy Au−Ge nanoparticle; (f) Au−Ge binary alloy phase diagram.[21] The solid gray curves represent the Au and Ge liquidus and solidus lines, respectively. Squares represent measurements of the temperature-dependent Ge content of Au−Ge alloy drops at the tip of Ge NWs from the array in Figure 1. Inset: Schematic of the Au−Ge alloy drop sessile on the NW, illustrating the contact angle β decrease with increasing temperature, determined by the balance of forces (see text for details).

phase behavior. Modifying the free surfaces by termination with a graphitic carbon shell restores a nearly bulk-like phase diagram, emphasizing the importance of surface effects on the phase behavior of the nanoscale alloy.

Figure 1a shows a TEM image of one of the investigated linear arrays, consisting of 13 Ge NWs (of which the 10 central ones are shown) with systematically varying diameters on the original Ge(111) substrate. The NW diameters increase stepwise from both sides toward the center of the array, thus creating 6 pairs of NWs with identical diameters. Figures 1b shows bright-field TEM images, obtained at 420 °C, of segments close to the Au−Ge tip for six consecutive NWs labeled in Figure 1a (NW number 1 is outside the field of view). Apart from the systematic diameter variation, all NWs are identical in structure: they are monocrystalline with axis along the [111] direction, and have Au-rich alloy melt drops at the tips, clearly distinguished by their darker contrast. The liquid Au−Ge alloy drops have identical shapes and interfaces to the NWs. The drops are truncated spheres with diameters ~10% larger than those of the NWs themselves, consistent with the surface energies and the force balance of the liquid−vapor−solid trijunction.[16]

Figure 2a−e shows the evolution of one NW in the linear array (Figure 1, NW 3, 42 nm) during heating from room temperature to 575 °C. Initial heating to 300 °C, where the Au−Ge particle at the NW tip is still solid, desorbs the native oxide from the Ge surface.[13,20] Surface melting of the alloy particles, which occurs gradually above 350 °C, is followed by the melting of the entire nanoparticle[13] close to the bulk eutectic temperature, T_E, as the alloy achieves the (eutectic) composition with the lowest melting point by uptake of Ge from the NW. Above 380 °C, all alloy particles are liquid. A further increase in temperature to 575 °C ($\gg T_E$) is accompanied by a continuous increase of the volume of the now liquid alloy drops and receding of the interface between the drop and the adjacent solid Ge NW, as shown in Figure 2b−e. Between room temperature and 575 °C, the interface in this particular NW draws back by ~70 ± 2 nm. Ge uptake into the alloy drop increases its volume and shifts its composition toward higher Ge content. We use measurements of the drop volume to quantify the alloy composition as a function of temperature for drops with different sizes, following a procedure described earlier[13] (see Methods for details). In equilibrium, the composition of the drop traces the liquidus of the nanoscale system—the Au−Ge alloy drop in contact with the solid Ge NW—involved in VLS growth. Figure 2f compares the measured liquidus for several of the NWs in the array (30−70 nm diameter) and one thicker NW (284 nm diameter) on the same sample, with the bulk phase diagram of the Au−Ge binary system.[21]

The nanometer-sized Au−Ge seed drops used in the VLS growth of Ge NWs generally show substantially lower liquidus temperatures than a bulk Au−Ge alloy, consistent with our earlier results.[13] The depression of the nanoscale liquidus implies a Ge content and volume of the VLS seed drop much larger than predicted by the bulk phase diagram.[21,22]

Simultaneous measurements on NWs with different diameters, presented here, allow us for the first time to observe and quantify the pronounced size dependence of this phase behavior. Figure 2f clearly shows the primary characteristic of this size dependence: smaller drops at the tips of thin NWs systematically show a higher equilibrium Ge concentration than their larger counterparts.

Since both the Au−Ge alloy drops and Ge NWs have spatial dimensions in the nanometer range, excess energies due to free surfaces and interfaces can no longer be neglected but become comparable to the "bulk" contributions to the total free energy.[16] In the particular geometry considered here (*i.e.*, a nanowire), the phase diagram of the nanoscale system is modified from the corresponding bulk phase diagram primarily due to the factor $2\sigma_{sv}/R_s$, given by the surface tension, σ_{sv}, and radius R_s of the solid NW.[16] The surface energies of the liquid drop (surface tension σ_{lv}) and the solid−liquid interface, σ_{ls}, as well as the molar volumes and surface forces, while not negligible, tend to be small. The presence of a free surface leads to a progressive destabilization of wires with small diameters. Hence, as the temperature is increased, thinner wires will more readily transfer Ge into the Au−Ge drop than thicker ones. In addition, there is a second size-dependent effect on the Ge solubility due to the surface tension, σ_{lv}, of the liquid alloy drop itself. Overall, the two surface terms tend to destabilize the solid NW and stabilize the liquid alloy drop, causing a shift of the equilibrium Ge content of the drop to substantially higher values than in the bulk. While additional investigations are necessary to fully understand the atomistic behavior of the liquid alloy as a function of temperature, the observed size dependence of the equilibrium Ge concentration along the liquidus is in agreement with the predictions based on the thermodynamics of finite-sized systems[16] that predict a strong size dependence, albeit only for thinner NWs with diameters below 30 nm.

Further support for the above scenario is obtained by analyzing the shape of the Au−Ge alloy drop, which changes markedly as the temperature is increased. The equilibrium geometry of a drop at the tip of a NW is determined by a balance of forces, described by the modified Young equation, $\sigma_{lv}\cos\beta = \sigma_{sv}\cos\alpha - \sigma_{ls} - (\tau/r)$.[23] Here, τ is the line tension and r the radius of the solid−liquid interface, and β denotes the contact angle. For the wire geometry, $\alpha = 90°$ (inset of Figure 2f), and estimated values of τ/r are negligible compared to the other surface energies due to the small line tension ($\tau \sim 10^{-9}$ J/m[23]). Hence, the equation simplifies to $\sigma_{lv}\cos\beta \approx -\sigma_{ls}$. For macroscopic Au−Ge drops on extended planar Ge surfaces, the contact angle β decreases with increasing temperature along the (bulk) liquidus, as σ_{ls} decreases at higher temperatures while the interfacial tension σ_{lv} is approximately constant

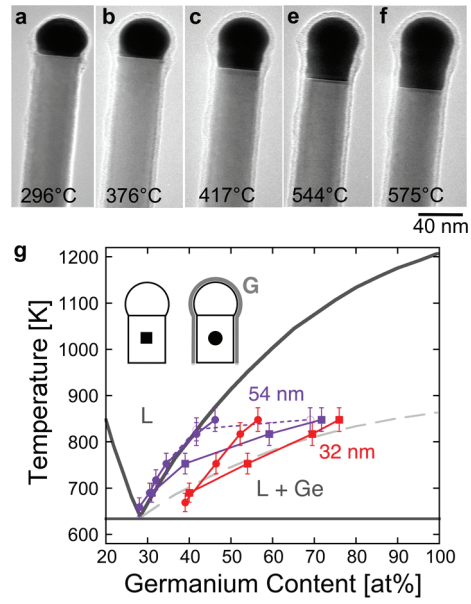

Figure 3. (a−f) Sequence of TEM images showing a Ge NW from a linear array of NWs encapsulated in carbon shells during *in situ* annealing at different temperatures between room temperature and 575 °C. (a) Initial *in situ* assembly of the C shell. (b−f) Exchange of material across the Ge NW/liquid drop interface after the assembly of the shell and the melting of the alloy Au−Ge nanoparticle. (g) Comparison of the liquidus for NWs with and without C shells, full circles and full squares, respectively (see inset), for two different diameters.

over the entire Ge-rich part of the phase diagram.[24] The wetting observed between our nanoscale Au−Ge drops and Ge NWs shows the same behavior; that is, the contact angles become progressively smaller at higher temperatures, which gives rise to the particular drop shapes—changing from spherical toward ellipsoidal—at elevated temperatures (TEM: Figures 2a−e; schematic: inset of Figure 2f). Young's equation therefore implies that the surface tension of the drops, σ_{lv}, indeed decreases along the liquidus to higher temperature and Ge concentration, as assumed above, contributing to stabilizing the liquid drop and driving its unusually high Ge uptake observed experimentally.

An immediate consequence of the deviations of the phase behavior of the nanoscale Au−Ge system from the bulk phase diagram is the notion that the alloy liquidus could be tuned by judicious changes in surface termination, that is, altering either the surface tension of the solid NW (σ_{sv}) or that of the alloy melt drop (σ_{lv}). We have explored this possibility by further *in situ* observations, again on linear arrays of Ge NWs subjected to identical conditions, but now considering NWs whose surface is covered by a thin graphitic carbon shell. Carbon shells encapsulating the entire Ge NWs were assembled *in situ* according to the procedure described in refs 20 and 25. Figure 3a−f follows the evolution during annealing of one NW, again part of a linear array as the one shown in Figure 1. The NW shown in Figure 3a−f has a diameter identical to the wire

shown in Figure 2a−e (42 nm), but its entire surface is covered by a thin (~ 5 nm) C shell. Above 365 °C, surface melting develops gradually and leads to the melting of the entire alloy seed drop at 386 °C. With further increase in temperature, the solid−liquid interface moves into the Ge NW, similar to the behavior observed for uncoated NWs. However, upon heating to 575 °C, the interface has receded only 30 ± 2 nm, significantly less than for an identical NW without a C shell (Figure 2e). The same behavior, a reduced Ge solubility compared to uncoated NWs with the same diameter at the same temperature, was observed for all C-terminated NWs in the array. A comparison of the measured liquidus lines for two other NWs with and without a C shell is shown in Figure 3g. For the C-terminated NWs, we again find a systematic diameter-dependent liquidus similar to NWs without shells; that is, for the same temperature, the Ge content along the liquidus is generally higher for NWs with smaller diameter. However, the overall solubility of Ge in the melt drop is reduced. For the larger (54 nm diameter) NW, the solubility is indeed comparable to the bulk. Strikingly, at temperatures above 550 °C, most of the C-terminated NWs can adjust their composition abruptly, within few seconds, to accommodate significantly more Ge. When this adjustment occurs, the Ge interface recedes rapidly and the volume (and hence Ge content) of the alloy melt drop increases close to that of NWs with free surfaces, as shown in Figure 3g (dashed line) for one of the 54 nm NWs.

There are two possible explanations for the modified behavior of C-terminated Ge NWs, a raised, nearly bulk-like Au−Ge liquidus, and the sudden jump at high temperature toward the suppressed liquidus of NWs with free surfaces. Encapsulation in a C shell can alter the thermodynamics of the system, effectively simulating a bulk-like environment of the NW and alloy drop if the C sheets wet their surfaces and the corresponding interface energies are small. The sudden transition to the free liquidus (*i.e.*, enhanced Ge uptake of the alloy melt) could then accompany a spontaneous dewetting from the C shell, that is, restoration of surface energies similar to those of free NWs. A second possibility, the existence of kinetic constraints due to the C-termination preventing the NW drop system from reaching equilibrium, for example, by pinning the solid−liquid interface by stress, cannot be excluded on the basis of our current observations. In this scenario, a sudden depinning could allow the system to equilibrate rapidly, that is, restore the liquidus of the free NW. Irrespective of the precise origin of the modifications induced by C surface termination, our observations emphasize that C-encapsulated NWs, used recently as a platform for studying nanoscale diffusion processes,[26] are complex systems with their own distinct properties and cannot generally be used as models to study the physics of semiconductor NWs.

In conclusion, we have used *in situ* TEM experiments on liquid Au−Ge alloy drops at the tips of Ge NWs, arranged in arrays with systematic variations in NW diameter, to determine the size-dependent equilibrium composition of the nanoscale Au−Ge alloy drops. We establish that the liquidus of the nanoscale system deviates significantly from the bulk phase diagram and shows a pronounced size dependence in the form of a progressive depression of the liquidus (or increase of the liquidus Ge concentration for the same temperature) with decreasing NW and drop diameters. Our results are primarily relevant to VLS growth of NWs, which operates along (or close to) the liquidus line of the binary alloy. Although NW growth by a vapor−solid−solid (VSS) mechanism has also been reported, VLS growth is usually preferred, particularly for group IV semiconductors, as it provides high and predictable growth rates, and the prospect of doping and the growth of alloys *via* the liquid catalyst drop. Our measurements of the nanoscale binary phase diagram show that the liquidus is progressively moved to lower T as the diameter of wire and drop decreases. In other words, small drops at the tip of thin nanowires have much higher equilibrium Ge content than would be predicted by the bulk phase diagram. Since the drop diameter determines the diameter of the growing wire, knowledge of the drop composition is key to controlling VLS growth. For example, using annealing to absorb additional Ge into the drop, and hence increase its diameter, controlled diameter changes can be achieved along the length of a VLS nanowire.[13] In addition, knowledge of the amount of dissolved Ge is important for the growth of sharp heterojunctions, that is, to devise approaches to switch from one semiconductor species to another (*e.g.*, from Ge to Si) while producing a sharp junction with minimal intermixing. As shown in our work, lithographic techniques can be used successfully to produce catalysts for the growth of NWs with controlled diameter, making the use of such specialized growth protocols—optimized according to the phase diagram of a specific diameter—feasible. The determination of the size-dependent phase behavior of the nanoscale binary alloy, achieved here, is also an important step toward clarifying the more complex behavior of ternary alloys, key to understanding the mechanisms of doping and of the growth of a broader class of compound semiconductors by the VLS mechanism. The behavior of nanoscale ternary alloys will be key to developing doping strategies, in which a dopant is incorporated from a liquid ternary alloy VLS drop,[27] thus ensuring homogeneous doping of the growing NW rather than a conformal deposition of a doped shell around it.[28] Our demonstration of the tuning of the liquidus by termination of the NW surface, fi-

nally, points to future strategies for the controlled manipulation of the phase behavior of NW/VLS drop systems by judiciously changing the specific surface free energies of the NW or drop, for example, by surfactants or controlled surface reactions, during nanowire growth.

METHODS

High-Temperature TEM of Nanoscale Au−Ge Drops. Variable-temperature TEM experiments were carried out in FEI Titan Cs-corrected environmental TEM and in JEOL JEM 2100F field emission microscope, both equipped with a Gatan 652 high-temperature sample holder. The *in situ* experiments cover the temperature range between room temperature and 600 °C at pressures below 10^{-7} Torr. The electron irradiation intensity was kept intentionally low (<0.1 A/cm^2) during observations to prevent any uncontrolled electron beam induced structural changes. Ordered arrays of Ge NWs with controlled diameter were grown by chemical vapor deposition on Ge(111) substrates, using electron-beam lithography patterned Au dots with diameters between 20 and 100 nm as growth seeds. Samples with a large distribution of NW diameters were grown by low-temperature thermal evaporation.[3] The TEM samples were prepared by precision mechanical thinning of the Ge substrate beneath linear arrays of Ge NWs to a thickness of ~5 μm and then mounted in the high-temperature holder with the nanowire array perpendicular to the incident electron beam. The intact Ge substrate ensured a uniform heat distribution and identical conditions, such as temperature, electron beam exposure, *etc.*, for the entire array. Ordered carbon shells were assembled on the surface of the Ge NWs following the procedure described in detail in ref 20. Briefly, in the presence of carbon (here deposited *ex situ*), the Au in the catalyst particle, and small Au aggregates on the nanowire surface drive the complete encapsulation of the nanowire and the Au-rich tip in a multilayer shell of graphene fragments.

The Au−Ge alloy composition as a function of temperature was quantified from measurements of the drop volume.[13] The Ge content, N_{Ge}, was calculated from the volume of the alloy drop, $V(T)$, according to $N_{Ge} = (V(T) - N_{Au}v_{Au})/v_{Ge}$, where N_{Au} is the (constant) number of Au atoms in the drop and v_{Au} and v_{Ge} denote the atomic volumes of the alloy components, determined from the densities of liquid Au ($\rho_{Au} = 17.4 \times 10^3$ kg/m^3) and Ge ($\rho_{Ge} = 5.49 \times 10^3$ kg/m^3), respectively. *In situ* energy-dispersive X-ray spectrometry was used to determine the composition of the different size drops close to the eutectic point, which was assumed to be achieved upon the original melting of the nanoparticles at the tips of the NWs.[13]

Acknowledgment. We thank Dr. T. Picraux and Dr. S. Dayeh for the linear arrays of Ge nanowires and for insightful discussions. We are grateful to K. Kisslinger for technical support. Work was performed under the auspices of the U.S. Department of Energy under Contract No. DE-AC02-98CH1-886.

REFERENCES AND NOTES

1. Duan, X. F.; Lieber, C. M. General Synthesis of Compound Semiconductor Nanowires. *Adv. Mater.* **2000**, *4*, 298–302.
2. Kamins, T. I.; Li, X.; Williams, R. S. Growth and Structure of Chemically Vapor Deposited Ge Nanowires on Si Substrates. *Nano Lett.* **2004**, *4*, 503–506.
3. Sutter, E.; Ozturk, B.; Sutter, P. Selective Growth of Ge Nanowires by Low-Temperature Thermal Evaporation. *Nanotechnology* **2008**, *19*, 435607–435612.
4. Wagner, R. S.; Ellis, W. C. Vapor−Liquid−Solid Mechanism of Single Crystal Growth. *Appl. Phys. Lett.* **1964**, *4*, 89–91.
5. Thelander, C.; Agrawal, P.; Brongersma, S.; Eymery, J.; Feiner, L. F.; Forchel, A.; Scheffler, M.; Riess, W.; Ohlsson, B. J.; Gösele, U.; Samuelson, L. Nanowire-Based One-Dimensional Electronics. *Mater. Today* **2006**, *9*, 28–33.
6. Yan, R.; Gargas, D.; Yang, P. D. Nanowire Photonics. *Nat. Photonics* **2009**, *3*, 569–576.
7. Lewis, N. S. Toward Cost Effective Solar Energy Use. *Science* **2007**, *315*, 798–801.
8. Tian, B.; Kempa, T. J.; Lieber, C. M. Single Nanowire Photovoltaics. *Chem. Soc. Rev.* **2009**, *38*, 16–24.
9. Peng, K.; Xu, Y.; Wu, Y.; Yan, Y.; Lee, S.-T.; Zhu, J. Aligned Single-Crystalline Si Nanowire Arrays for Photovoltaic Applications. *Small* **2005**, *1*, 1062–1067.
10. Lin, Y.; Dresselhaus, M. S. Thermoelectric Properties of Superlattice Nanowires. *Phys. Rev. B* **2003**, *68*, 075304–075317.
11. Hochbaum, A. I.; Chen, R.; Delgado, R. D.; Liang, W.; Garnett, E. C.; Najarian, M.; Majumdar, A.; Yang, P. Enhanced Thermoelectric Performance of Rough Silicon Nanowires. *Nature* **2008**, *451*, 163–167.
12. Cui, Y.; Lauhon, L. J.; Gudiksen, M. S.; Wang, J.; Lieber, C. M. Diameter-Controlled Synthesis of Single-Crystal Silicon Nanowires. *Appl. Phys. Lett.* **2001**, *78*, 2214–2216.
13. Sutter, E.; Sutter, P. Phase Diagram of Nanoscale Alloy Particles Used for Vapor−Liquid−Solid Growth of Semiconductor Nanowires. *Nano Lett.* **2008**, *8*, 411–414.
14. Yang, J. E.; Jin, Ch. B.; Kim, Ch. J.; Jo, M. H. Band-Gap Modulation in Single Crystalline SiGe Nanowires. *Nano Lett.* **2006**, *6*, 2679–2684.
15. Delley, B.; Steigmeier, E. F. Size Dependence of Band Gaps in Silicon Nanostructures. *Appl. Phys. Lett.* **1995**, *67*, 2370–2372.
16. Schwalbach, E. J.; Voorhees, P. W. Phase Equilibrium and Nucleation in VLS-Grown Nanowires. *Nano Lett.* **2008**, *8*, 3739–3745.
17. Sa, I.; Lee, B.-M.; Kim, C.-J.; Jo, M.-H.; Lee, B.-J. Thermodynamic Analysis for the Size Dependence of $Si_{1-x}Ge_x$ Nanowire Composition Grown by Vapor−Liquid−Solid Method. *CALPHAD: Comput. Coupling Phase Diagrams Thermochem.* **2008**, *32*, 669–674.
18. Adhikari, H.; Marshall, A. F.; Goldthorpe, I. A.; Chidsey, C. E. D.; MacIntyre, P. C. Metastability of Au−Ge Liquid Nanocatalysts: Ge Vapor−Liquid−Solid Nanowire Growth Far below the Bulk Eutectic Temperature. *ACS Nano* **2007**, *1*, 415–422.
19. Vallee, R.; Wautelet, M.; Dauchot, J. P.; Hecq, M. Size and Segregation Effects on the Phase Diagrams of Nanoparticles of Binary Systems. *Nanotechnology* **2001**, *12*, 68–74.
20. Sutter, E.; Sutter, P. Au-Induced Encapsulation of Ge Nanowires in Protective Carbon Shells. *Adv. Mater.* **2006**, *18*, 2583–2588.
21. Predel, B. Phase Equilibria. In *Crystallographic and Thermodynamic Data of Binary Alloys - Electronic Materials and Semiconductors*; Madelung, O., Ed.; Springer: Berlin, 1998; Vol. 5.
22. Wang, J.; Leinenbach, C.; Roth, M. Thermodynamic Description of the Au−Ge−Sb Ternary System. *J. Alloys Compd.* **2009**, *485*, 577–582.
23. Schmidt, V.; Senz, S.; Gösele, U. The Shape of Epitaxially Grown Si Nanowires and the Influence of the Line Tension. *Appl. Phys. A: Mater. Sci. Process.* **2005**, *80*, 445–450.
24. Naidich, Y. V.; Perevertaila, V. M.; Obushchak, L. P. Contact Properties of the Phases Participating in the Crystallization of Gold−Silicon and Gold−Germanium Melts. *Poroshk. Metall.* **1971**, *151*, 63–67.
25. Sutter, P.; Sutter, E. Dispensing and Surface-Induced Crystallization of Zeptoliter Liquid Metal-Alloy Drops. *Nat. Mater.* **2007**, *6*, 363–366.
26. Holmberg, V. C.; Panthani, M. G.; Korgel, B. A. Phase Transitions, Melting Dynamics and Solid-State Diffusion in a Nano Test Tube. *Science* **2009**, *326*, 405–407.
27. Sutter, E.; Sutter, P. Vapor−Liquid−Solid Growth and Sb Doping of Ge Nanowires from a Liquid Au−Sb−Ge Ternary Alloy. *Appl. Phys. A: Mater. Sci. Process.* **2010**, *99*, 217–221.
28. Perea, D. E.; Hemesath, E. R.; Schwalbach, E. J.; Lensch-Falk, J. L.; Voorhees, P. W.; Lauhon, L. J. Direct Measurement of Dopant Distribution in an Individual Vapor−Liquid−Solid Nanowire. *Nat. Nanotechol.* **2009**, *4*, 315–319.